ELSEVIER

PII: S0032-3861(97)10331-7

Polymer Vol. 39 No. 20, pp. 4915–4921, 1998

0032-3861/98/$19.00+0.00

Mathematical modelling of thermoplastic natural rubber melt flow in a double feed extrusion system

Che Husna Azhari*, Jaafar Sahari and Li Qing
Department of Mechanical and Materials Engineering, Universiti Kebangsaan Malaysia, 43600 Bangi, Selangor, Malaysia
(Received 11 December 1995; revised 13 May 1997; accepted 24 November 1997)

A mathematical model for investigating the melt flow behaviour of thermoplastic natural rubber (TPNR) in a double feed system of a single-screw reciprocating injection unit using a specially written software is presented. The model enabled the prediction of processing parameters in the feed and main extruders, from which the optimum conditions for processing TPNR were obtained. The introduction of the double feed system also contributed to better mixing in the main extruder. © 1998 Elsevier Science Ltd. All rights reserved.

(Keywords: thermoplastic natural rubber; melt flow behaviour; extrusion)

INTRODUCTION

The current interest in polymer alloys and blends is, to a large extent, concerned with the dispersion and mixing of polymers on melt compounding processing equipment such as extruders[1]. Much of this work centred on controlling microstructure at will for a wide range of systems under melt processing conditions. Another interest is the analysis of melt flow behaviour, particularly for thermoplastic polymers in single-screw extruders. After the pioneering work of Tadmor *et al.*[2], other researchers have produced mathematical models to describe such behaviour[3–8].

An area which needs further development is the investigation of the melt flow behaviour during processing of a class of thermoplastic polymers known as thermoplastic natural rubbers (TPNRs). These polymer blends/alloys consist of thermoplastics, such as polypropylene (PP), alloyed with natural rubber (NR) with different thermoplastic to NR ratios. The rationale of producing such blends was to harness the desirable properties of NR and the processability of thermoplastics. The work on TPNRs has been done predominantly by Elliott[9–11]. The TPNR developed has since been commercialized as Vitacom™. Much of the published work on TPNRs to date has concentrated on their blend formulations in static mixing and correlating these with the ensuing morphology, as well as mechanical properties[9–13]. The only work describing melt flow behaviour of TPNR (PP/NR) blends has been that of Kuriakose and De[14]. In the Kuriakose and De study, the melt flow behaviour was evaluated in terms of rheological properties.

In this particular study, two issues are addressed: (i) the melt flow behaviour of TPNRs in melt processing and (ii) the feeding of blends in the pre-plastication stage. The blends were fed into the feed extruders prior to plastication in the main extruder. The schematics of this set-up are explained further in the mathematical model, in which the modifications to the original machine configuration are explained (see *Figure 1*).

* To whom correspondence should be addressed

MATHEMATICAL MODEL

Feed extruder

The feed extruders were divided into two sections: (a) the solids conveying section and (b) the melting section, as shown in *Figure 2*. The 'Maddock melting mechanism', as shown in *Figure 3*, was used in the analysis of the feed extruder, which was presented by Tadmor and Gogos[15]. In the present study, their analysis was used to predict the melting rate and the upper melt film thickness profiles along the feed extruder axis, and the amount of unmelted polymer at the end of the feed extruder. This information was subsequently used to determine the initial conditions of the main extruder.

Assuming the down-channel velocity of a solid bed as V_{sz}, the relationship of the rate of melting, $w_L(z)$, solid-bed width, X, and material properties is as follows[10]:

$$w_L(z) = \left\{ \frac{V_{bx}\rho_m U_2 \left[k_m(T_b - T_m) + U_1/2\right] X}{2\left[\lambda^* + C_m\left(\underline{T_b} - T_m\right)\overline{T^*}\right]} \right\}^{1/2} \quad (1)$$

where V_{bx}, k_m, ρ_m, T_b, T_m, T^*, C_m, U_1, U_2 and λ^* are the cross-channel directional barrel velocity, thermal conductivity, melt density, barrel temperature, melting point, the dimensionless mean temperature, the specific heat of melt polymer, the reduction of the rate of melt removal of the film by drag flow as a result of temperature dependence and shear thinning of the viscosity, the rate of viscous dissipation (per unit width) in the melt film and latent heat of fusion, respectively. The film thickness δ is given as:

$$\delta = \left\{ \frac{\left[2k_m(T_b - T_m) + U_1\right] X}{V_{bx}U_2\rho_m\left[\lambda^* + C_m\overline{T^*}(T_b - T_m)\right]} \right\}^{1/2} \quad (2)$$

The initial dimensions of five zones were determined from

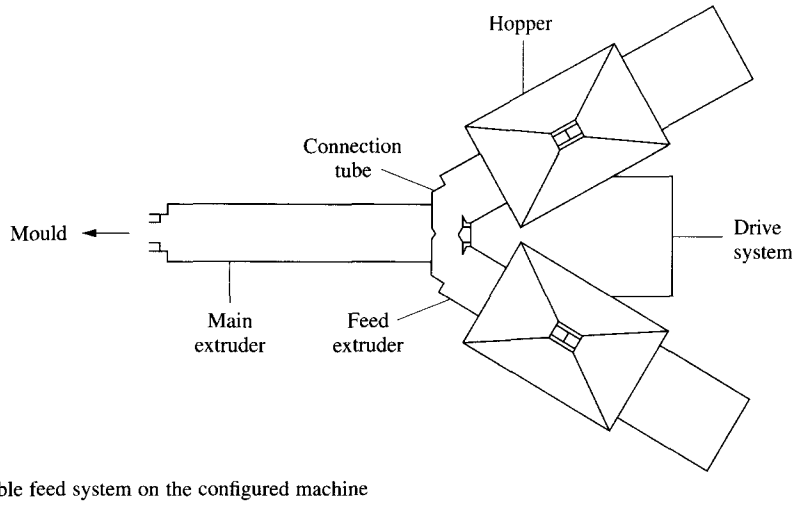

Figure 1 Top view of the double feed system on the configured machine

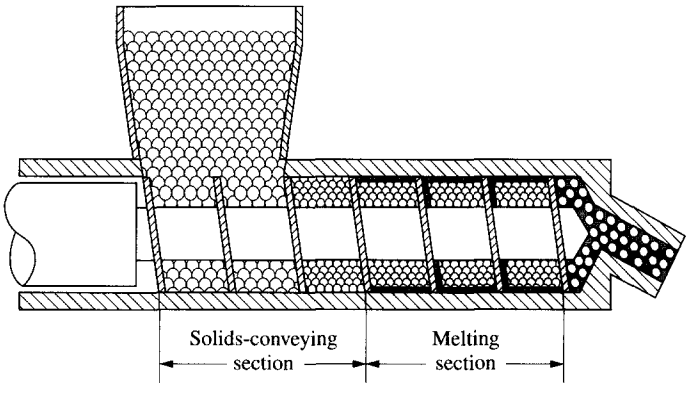

Figure 2 Schematic of the feed extruder

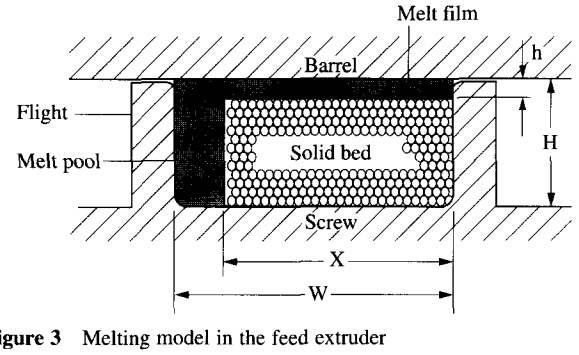

Figure 3 Melting model in the feed extruder

the following expressions:

$$W_{B0} = H_{C0} = H_{E0} = \frac{W(1-R)}{RWH/\pi R_p^2 - 1} \tag{3}$$

$$R = k_A R_A + k_B R_B \tag{4}$$

where k_A, k_B, W, H, R_p, R_A and R_B are the ratio of the PP component to the PP/NR blend, the ratio of the NR component to the PP/NR blend, the channel width, the channel depth, the mean radius of solids, and the amount of unmelted polymeric PP and NR, respectively.

Main extruder

The main extruder was divided into two sections with respect to its functions: (a) the mix-melting section and (b) the melt-conveying section, as shown in *Figure 4*. The locations of these sections along the screw axes depend upon the operating conditions, and therefore usually do not coincide with those of the geometrical sections. The mix-melting section was divided into five zones, as shown in *Figure 5*: (A) a dispersive solid–melt bed; (B) a melt pool; (C) a melt film between the barrel surface and the solid–melt bed; (D) a melt film between the screw surface and the solid–melt bed; and (E) a melt film between the screw flight and the solid–melt bed. Before the computation was effected, the following assumptions were presumed to hold true: (1) steady-state conditions prevailed; (2) the screw channel could be described by a local Cartesian system; (3) the melting region consisted of five distinct regions; (4) the polymer had a sharp melting point, T_m; (5) The down-channel velocity of the solid–melt bed varied with z; (6) the molten polymer was purely viscous; (7) the solid-melt interfaces were smooth and were at determinate physical conditions; (8) leakage flow from the flights could be neglected. Additional assumptions are given at the point where they enter the analysis.

Zone A represents a solid–melt bed. The flow of thermal energy in the solid–melt bed is governed by the following expressions, assuming that $W_M \gg H_M$:

$$-\frac{V_{sy1}}{\alpha_s}\frac{\partial T_{s1}}{\partial y} + \frac{V_{Mz}}{\alpha_s}\frac{\partial T_{s1}}{\partial z} = \frac{\partial^2 T_{s1}}{\partial y^2} \quad a \le y \le H_s \tag{5}$$

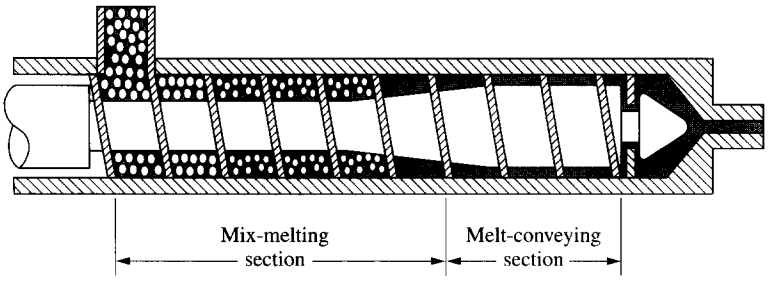

Figure 4 Schematic of the main extruder

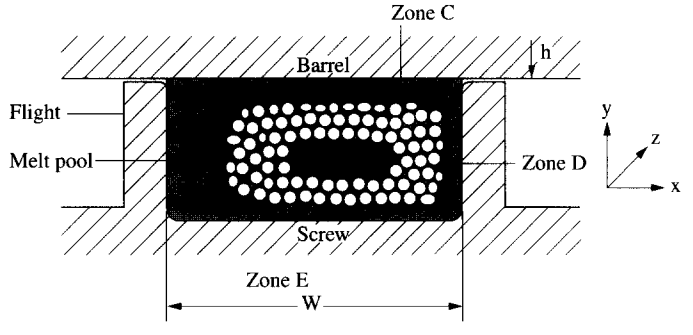

Figure 5 Melting model in the main extruder

$$\frac{V_{sy2}}{\alpha_s}\frac{\partial T_{s2}}{\partial y}+\frac{V_{Mz}}{\alpha_s}\frac{\partial T_{sz}}{\partial z}=\frac{\partial^2 T_{s2}}{\partial y^2}\quad 0\le y\le a^* \tag{6}$$

where α_s, V_{sy1}, V_{sy2}, T_{s1}, T_{s2} and H_M are the thermal diffusivity of the solid polymer, the effective radical movement of the interfaces AC and AE caused by melting, the temperature profiles in the solid–melt bed and the height of the solid–melt bed respectively; a^* is the distance measured from the bed floor at which the temperature gradients vanished and the temperature profiles matched, i.e.

$$T_{s1}(y=a^*,z)=T_{s2}(y=a^*,z) \tag{7}$$

$$V_{sy}(y=a^*)=0 \tag{8}$$

The solution of equations (5) and (6) may satisfy the following boundary conditions:

$$T=T_f \text{ at } z=0 \tag{9a}$$

$$T=T_m \text{ and } v_{sy}=-V_{sy2} \text{ at } y=0 \tag{9b}$$

$$T=T_m \text{ and } v_{sy}=V_{sy1} \text{ at } y=H_M \tag{9c}$$

where T_f is the average feed temperature of the mixtures coming from the two feed extruders. It is assumed that, at the start of melting in the main extruder, heat balance within feeds had been reached. T_f is estimated from:

$$T_f=(k_A T_{fA} C_{pA}+k_B T_{fB} C_{pB})/(k_A C_{pA}+k_B C_{pB}) \tag{10}$$

where k, C_p and T_{fi} are the ratio of each component to the blend, the heat capacity and mean temperature of each component, respectively. The subscripts A and B denote the two components of the blend.

The down-channel solid–melt bed velocity V_{Mz} is estimated from the local flow rate and dimensions of the solid–melt bed, i.e.

$$V_{Mz|z}=\frac{mA_{|z}}{\rho_M W_{M|z} H_{M|z}} \tag{11}$$

where $W_{M|z}$ and $H_{M|z}$ are the width and height, respectively, of the solid–melt bed at the down-channel position z.

Zone B represents a melt pool. The flows were considered to be fully developed and low viscous dissipation prevailed in the slowly growing melt pool bounded by walls of constant temperature. The transverse flow may be approximated by:

$$\frac{\partial P^{(B)}}{\partial x}=\frac{\partial}{\partial y}\left(\eta_x^{(B)}\frac{\partial v_x^{(B)}}{\partial y}\right) \tag{12}$$

The down-channel flow field is described by:

$$\frac{\partial P^{(B)}}{\partial z}=\frac{\partial}{\partial x}\left(\eta^{(B)}\frac{\partial v_z^{(B)}}{\partial x}\right)+\frac{\partial}{\partial y}\left(\eta^{(B)}\frac{\partial v_z^{(B)}}{\partial y}\right) \tag{13}$$

The molten polymer was assumed to follow a power-law model, and the viscosity is given by:

$$\eta^{(B)}=m_0\exp\left[b\left(T_R-T^{(B)}\right)\right]\times\left[\left(\frac{\partial v_x^{(B)}}{\partial y}\right)^2+\left(\frac{\partial v_z^{(B)}}{\partial x}\right)^2+\left(\frac{\partial v_z^{(B)}}{\partial y}\right)^2\right]^{(n-1)/2} \tag{14}$$

where m_0, b, T_R and n are the power-law constant, the temperature sensitivity, the reference temperature and the power-law index, respectively.

The energy equation is given as:

$$\rho_m^{(B)} C_p^{(B)} v_z^{(B)}\frac{\partial T^{(B)}}{\partial z}=k_m^{(B)}\left(\frac{\partial^2 T^{(B)}}{\partial x^2}+\frac{\partial^2 T^{(B)}}{\partial y^2}\right)+\eta^{(B)}\left[\left(\frac{\partial v_x^{(B)}}{\partial y}\right)^2+\left(\frac{\partial v_z^{(B)}}{\partial x}\right)^2+\left(\frac{\partial v_z^{(B)}}{\partial y}\right)^2\right] \tag{15}$$

The solution of equations (12), (13) and (15) satisfies the following boundary conditions:

$$v_z^{(B)} = 0,\ v_z^{(B)} = 0,\ T^{(B)} = T_c \text{ at } y = 0 \quad (16a)$$

$$v_z^{(B)} = V_{bz},\ v_x^{(B)} = -V_{bx},\ T^{(B)} = T_b \text{ at } y = H \quad (16b)$$

$$v_z^{(B)} = 0,\ T^{(B)} = T_c \text{ at } x = 0 \quad (16c)$$

$$v_z^{(B)} = V_{Mz},\ T^{(B)} = T_m \text{ at } x = W_M \quad (16d)$$

where T_c is the screw temperature, which is determined from the following empirical expression[11]:

$$T_c(z) = T_b[1 - \exp(\alpha z)] + T_f \exp(\alpha z) \quad (17)$$

where

$$\alpha = \ln[(T_m - T_b)/(T_f - T_b)]/Z' \quad (18)$$

with Z' the position at which the lower melt film begins to increase.

Zones C, D and E represent the thin melt films surrounding the solid–melt bed, as shown in *Figure 5*. Zone D can be treated as an extension of zone E. Assuming that flows are fully developed in the down- and cross-channel directions (i.e. $\partial v_x/\partial x = 0$ and $\partial v_z/\partial z = 0$) and that the melt films circulated around the solid–melt bed, the x- and z-components of the momentum equations become:

$$\frac{\partial P}{\partial x} = \frac{\partial}{\partial y}\left(\eta \frac{\partial v_x}{\partial y}\right) \quad (19)$$

$$\frac{\partial P}{\partial z} = \frac{\partial}{\partial y}\left(\eta \frac{\partial v_z}{\partial y}\right) \quad (20)$$

The viscosity, η, of the melt is given by:

$$\eta = m_0 \exp[b(T_R - T)]\left[\left(\frac{\partial v_z}{\partial y}\right)^2 + \left(\frac{\partial v_x}{\partial y}\right)^2\right]^{(n-1)/2} \quad (21)$$

The energy transport equation is given as:

$$\rho_m C_m v_z \frac{\partial T}{\partial z} = k_m \frac{\partial^2 T}{\partial y^2} + \eta\left[\left(\frac{\partial v_x}{\partial y}\right)^2 + \left(\frac{\partial v_z}{\partial y}\right)^2\right] \quad (22)$$

The boundary conditions for zone C were:

$$v_z^{(C)} = V_{Mz},\ v_x^{(C)} = 0,\ T = T_m \text{ at } y = H - H_C \quad (23a)$$

$$v_z^{(C)} = V_{bz},\ v_x^{(C)} = -V_{bx},\ T = T_b \text{ at } y = H \quad (23b)$$

and the boundary conditions for zones D and E were:

$$v_x^{(E)} = 0,\ v_z^{(E)} = 0,\ T^{(E)} = T_C \text{ at } y = 0 \quad (24a)$$

$$v_x^{(E)} = 0,\ v_z^{(E)} = V_{Mz},\ T^{(E)} = T_m \text{ at } y = H_E \quad (24b)$$

NUMERICAL SCHEME

The melting profiles in the feed extruder can be obtained by solving equations (1) and (2) numerically, using the Newton–Raphson method. In order to compute the velocity, the pressure and temperature distributions in the five zones along the main extruder, we numerically solved the system equations using the over-relaxation method. The computational algorithm that we have employed is very similar to that of Elbirli *et al.*[6], with the one important difference being that we have used an integration method to solve the equations of motion. In the present investigation, at each incremental axial position Δz, equations (12), (13), (19) and (20) were first solved for the velocity distributions in zones B, C, D and E, using the fourth-order Runge–Kutta method, subject to the boundary conditions in equations (16a–d), (23a and b) and (24a and b), respectively. The temperature distributions were then determined by rewriting equations (15) and (22) in finite difference form and solved using the Crank–Nicolson method.

It should be pointed out that the velocity and temperature distributions were coupled, making the numerical solution of system equations iterative in nature.

Table 1 Physical and thermal properties of polypropylene and natural rubber

Material	PP[a]	NR[b]
Properties in the solid state		
Density (kg m^{-3})	905	920
Specific heat, C_{ps} (J kg^{-1} °C^{-1})	2400	1881
Thermal conductivity, k_s (W m^{-1} °C^{-1})	0.235	0.192
Heat of fusion (J kg^{-1})	58 000	64 000
Melting point, T_m (°C)	170	80
Coefficients of friction	0.67	1.75
Properties in the molten state		
Density (kg m^{-3})	770	920
Specific heat, C_{pm} (J kg^{-1} °C^{-1})	3074	1881
Thermal conductivity, k_m (W m^{-1} °C^{-1})	0.182	0.134
Power-law index for viscosity, n	0.335	0.13
Power-law constant for viscosity, m_0 (Pa s^n)	15 100	292 800
Reference temperature, T_R (°C)	205	100
Temperature coefficient, b (K^{-1})	0.014	0.0201

[a]GSE 111 AA polypropylene grade (for general compounding) obtained from Polypropylene Malaysia
[b]SMR GP grade obtained in bale form (33 kg) from the Rubber Research Institute of Malaysia

Table 2 Extruder configurations[a]

Extruder	Unit	Main extruder	Feed extruder
Screw diameter	mm	30	30
Length in feed zone	L D^{-1}	10	10
Length in transition zone	L D^{-1}	5	—
Length in metering zone	L D^{-1}	5	—
Helix angle	degree	17.8	17.8
Channel width	mm	25.9	25.9
Channel depth in feed zone	mm	5	5
Channel depth in metering zone	mm	2.0	—
Flight width	mm	3.0	3.0
Flight clearance (radical)	mm	0.06	0.06
Screw lead	mm	30.38	30.38

[a]Extruder configurations were based on the Arburg 850-210 A 320D injection moulding machine originally equipped with a single-screw extruder

Table 3 Operating conditions

Extruder	Unit	Main extruder (TPNR)	Feed extruder (PP)	Feed extruder (NR)
Barrel temperature	°C	180–210	180–190	95–105
Screw temperature	°C	41.1–210	25	25
Average feed temperature	°C	41.1–57.6	25	25
Heating started from	turn	2	3	5
Screw speed	rpm	80–100	4.5–43.8	4.3–42
Throughout	kg h^{-1}	8.85–12.75	0.885–11.475	0.885–11.475

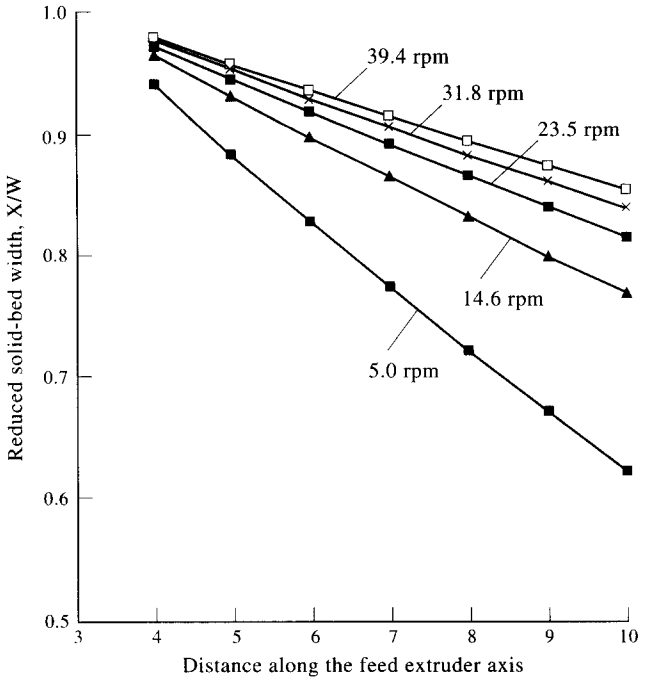

Figure 6 Effect of screw speed on the solid-bed width profiles of PP in the feed extruder

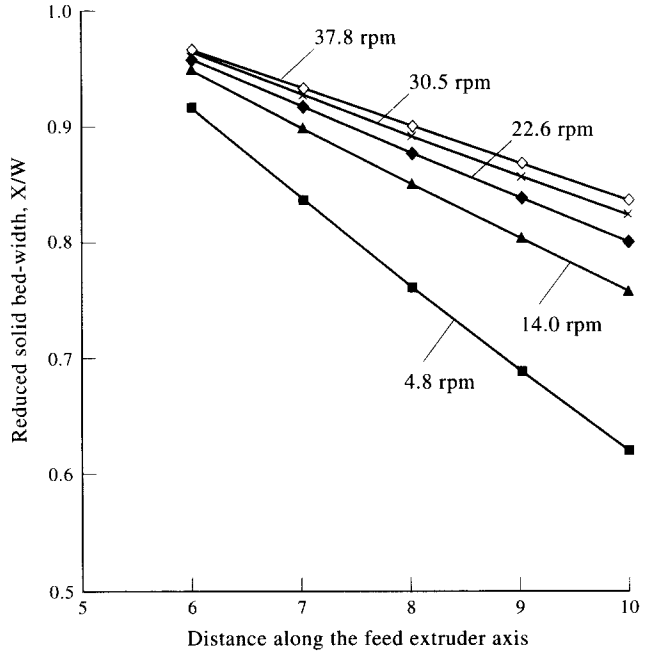

Figure 7 Effect of screw speed on reduced solid-bed width profiles of NR in the feed extruder

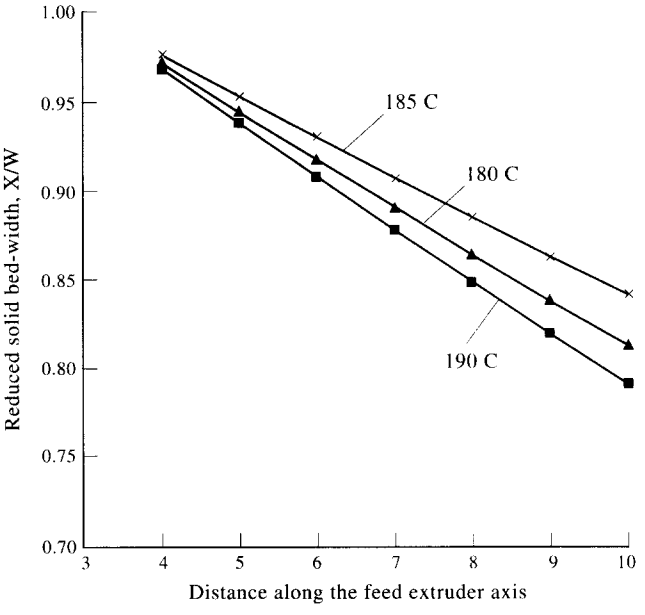

Figure 8 Effect of temperature on reduced solid-bed width profiles of PP in the feed extruder

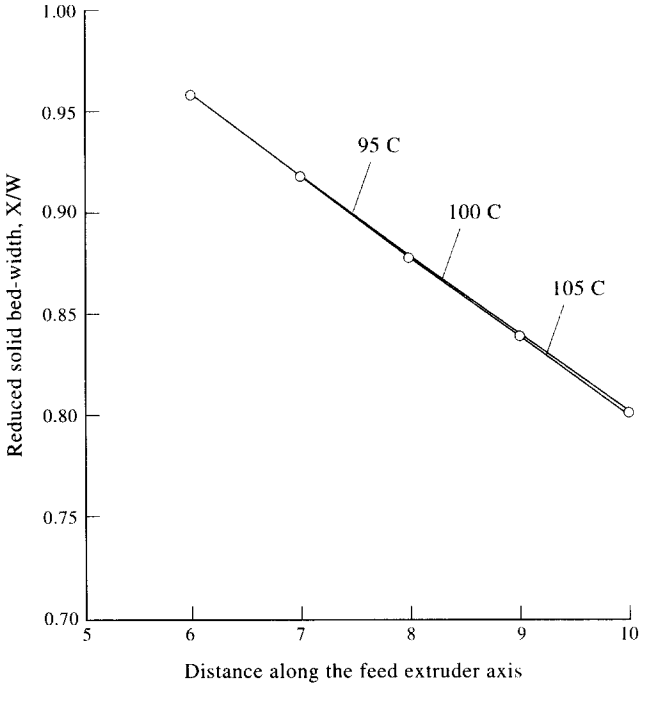

Figure 9 Effect of temperature on reduced solid-bed width profiles of NR in the feed extruder

RESULTS AND DISCUSSION

The TPNRs used in this study were PP/NR blends of 10:90, 30:70, 50:50, 70:30 and 90:10 ratios. The physical properties were determined from the following expression:

$$G_{AB} = k_A G_A + k_B G_B \tag{25}$$

and the rheological properties were estimated by:

$$\log \eta_{AB} = k_A \log \eta_A + k_B \log \eta_B \tag{26}$$

where G is a physical property such as density, specific heat, etc., k is the ratio of each component to the blend and η is the apparent shear viscosity. The subscripts A, B and AB denote PP, NR and PP/NR blends, respectively. The characteristics of the two basic materials are given in *Table 1*. *Tables 2* and *3* summarize, respectively, the extruder configurations and operating conditions which were employed in the simulation.

The whole mathematical model was based on the assumption that steady-state conditions prevailed. It was noted that the melting model taking into account the unsteady state has been developed by Pearson[16], but since the system equations were very complex, the steady-state model was adopted in this study.

The analysis in the feed extruder adopted Tadmor's model, bearing in mind the modified versions of Elbirli[6] and

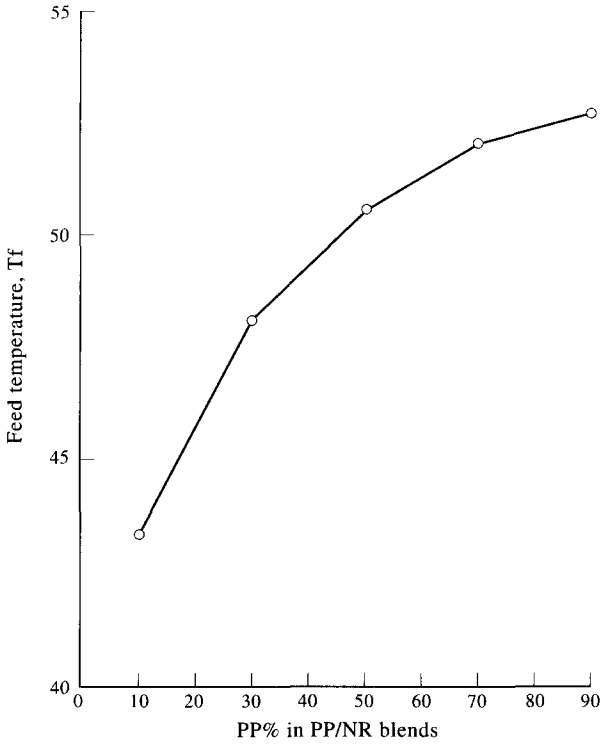

Figure 10 Plots of feed temperature *versus* increasing PP content in PP/NR blends

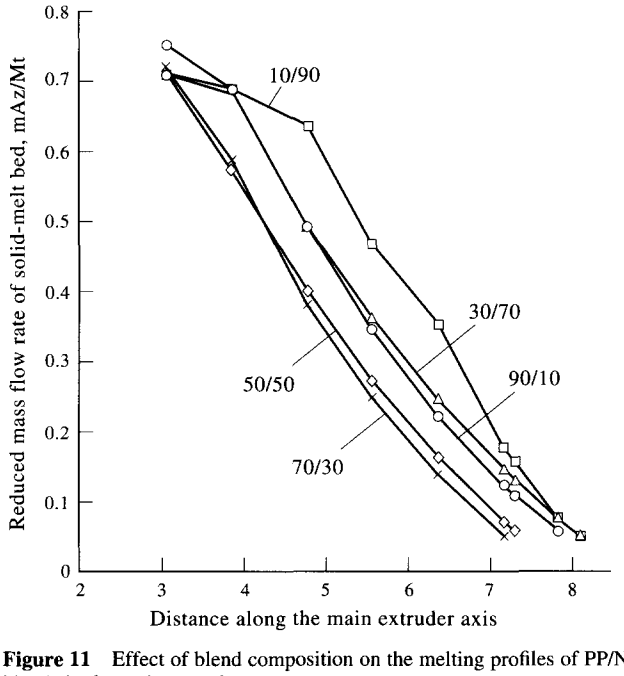

Figure 11 Effect of blend composition on the melting profiles of PP/NR blends in the main extruder

Cox and Fenner[17], which assumed that the solid bed was rigid. The parameter used was *X/W* (see *Figure 3*), which is the reduced solid-bed width. In this study, the geometry of the feed extruder was designed to give an *X/W* value reported to be in the range which can hold the Maddock melting mechanism[18,19], a value greater than 0.20.The results of the computation in the feed extruders are given in *Figures 6–9*. *Figures 6* and *7* give predictions of the effect of screw speed on the melting profiles of PP and NR in the feed extruders. It was seen that the amount of melted polymer increased with the screw speed. This was reasonable,

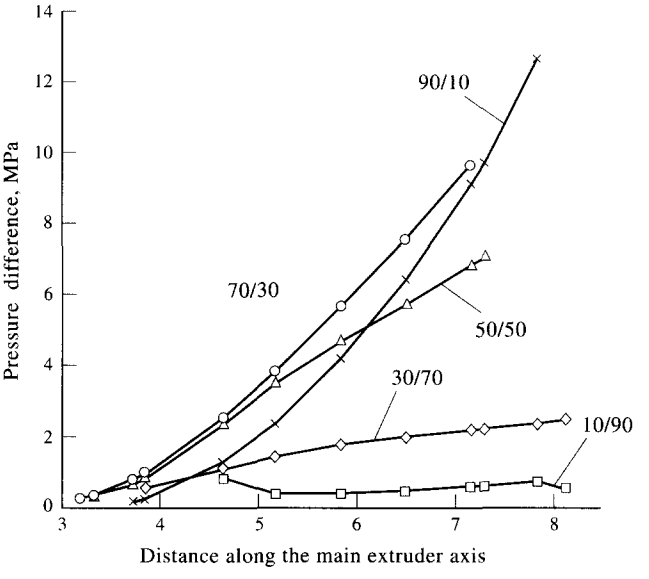

Figure 12 Effect of blend composition on the axial pressure profiles of PP/NR blends in the main extruder

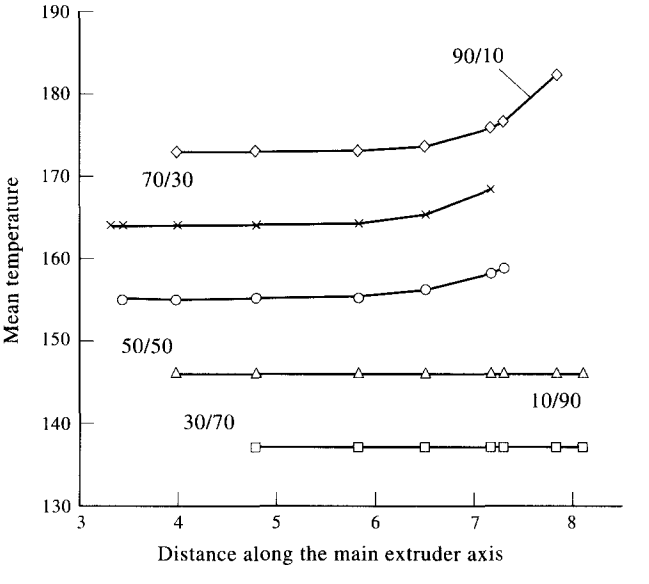

Figure 13 Effect of blend composition on the temperature profiles of TPNR melts in the main extruder

since smaller values of screw speed indicated longer residence times of the polymer in the extruder, allowing more time for the solid polymer to melt, resulting in a faster rate of decrease in the solid-bed width along the extruder axis. Due to the geometry of the extruder, the polymer was melted by heat from the hot barrel more than by viscous shear heating. A comparison of *Figures 6* and *7* led us to conclude that the effects of screw speed on the melting of PP and NR in the feed extruders were nearly identical.

Figures 8 and *9* give predictions of the effect of barrel temperature on the melting profiles of PP and NR in the feed extruders. As shown in *Figure 8*, even with a small change in barrel temperature (5°C), the effect on processing PP was significant. However, differences of barrel temperatures in the feed extruder did not seem to affect the reduced solid-bed width of NR along the extruder axis (*Figure 9*). This may be attributed to the following: (1) the thermal conductivity of NR was greater than that of thermoplastics and (2) the geometry of the feed extruder enabled a greater

volume of melt. A comparison between the two figures led us to conclude that the effect of barrel temperature on processing PP was much more significant than that of NR.

Figures 10–13 show the effect of blend composition on the processing of PP/NR blends. NR was fed at a temperature of 100°C, whilst PP was fed at 185°C. The temperature of the inlet of the main extruder was 185°C, with a screw speed of 90 rpm. It can be seen from *Figure 10* that the rate of increase in feed temperature decreased with an increase in PP content. *Figure 11* shows plots of reduced mass flow rate of the solid–melt bed, m_{Az}/M_t, where m_{Az} is the mass flow rate of the solid–melt bed in the z-direction and M_t is the total mass flow rate, *versus* distance along the main extruder axis for various PP/NR blends. When the melting was assumed to be essentially complete, i.e. when the value of m_{Az}/M_t became less than 0.05. It can be seen from *Figure 11* that the melting rates of PP/NR blends with 10:90 and 90:10 ratios were slower than those of other PP/NR blends. The large difference between the two composites of PP/NR blends was attributed to a relatively slower melting rate.

Figure 12 shows plots of axial pressure difference *versus* distance along the main extruder axis for various PP/NR blends. It was noted that the pressure in the melting section increased along the main extruder axis and the rate of increase in the axial pressure increased with PP content. To obtain the theoretical values of the axial pressure profiles, a constant value of melt density was used. In this respect, our results are similar to those of Lee[20]. Even though the melt density is known to vary with temperature, theoretically predicted axial pressure profiles obtained by Lee were found to be unchanged from those obtained with a constant value of melt density. This was attributed to the fact that the melt viscosity had a much stronger temperature dependency than the melt density. *Figure 13* shows, for a specified barrel temperature, T_b = 185/195/205°C, and screw speed N = 90 rpm, predicted average temperature profiles of TPNR melts along the extruder axis during the mix-melting process in the main extruder for various PP/NR blends. It was observed that the temperature changes of TPNR melts during melting increased with PP content. When the PP content in PP/NR blends was less than 50%, the processing characteristics of TPNR were more akin to those of elastomers, as the blends began to show the melt behaviour of elastomers.

CONCLUSIONS

It was inferred from the present study that both design and processing parameters influenced the amount of molten polymer in the system, measured as X/W, the reduced solid-bed width. Changes in screw speed in processing affected both PP and NR; the higher the screw speed, the greater the values of X/W. The value of X/W was affected more at higher screw speeds. This phenomenon was observed for both the feed and the main extruders. Blend compositions affected melt characteristics, the critical composition being a ratio of 50:50 (PP/NR). The introduction of the feed system enabled melting to be completed in the 'feed' section of the main extruder, resulting in a larger melt conveying zone. The larger melt conveying zone would enable the system to offer better mixing of the blends. Though not exhaustive, the computation provided a basis for the selection of optimum processing conditions for these interesting classes of materials.

ACKNOWLEDGEMENTS

We would like to thank the Malaysian Ministry of Science, Technology and Environment for providing the funds for this work through IRPA programme 2-07-03-02.

REFERENCES

1. Favis, B. D., *Can. J. Chem. Engng*, 1991, **69**, 619.
2. Tadmor, Z., Duvdevani, I. and Klein, I., *Polym. Eng. Sci.*, 1967, **7**, 198.
3. Donovan, R. C., *Polym. Eng. Sci.*, 1971, **11**, 247.
4. Edmondson, I. R. and Fenner, R. T., *Polymer*, 1975, **16**, 49.
5. Halmos, A. L., Pearson, J. R. A. and Trottnow, R., *Polymer*, 1978, **19**, 1199.
6. Elbirli, B., Lindt, J. T., Gittgetreu, S. R. and Baba, S. M., *Polym. Eng. Sci.*, 1984, **24**, 988.
7. Lee, K. Y. and Han, C. D., *Polym. Eng. Sci.*, 1990, **30**, 665.
8. Shapiro, J., Halmos, A. L. and Pearson, J. R. A., *Polymer*, 1976, **17**, 90.
9. Elliott, D. J., *NR Technol.*, 1981, **12**(3), 59.
10. Elliott, D. J., in *Development in Rubber Technology—3*, ed. A. Whelan and K. S. Lee. Applied Science, London, 1982.
11. Elliott, D. J., in *Thermoplastic Elastomers From Rubber–Plastic Blends*, ed. S. K. De and A. K. Bhowmick. Ellis Horwood, 1990, pp. 102–129.
12. Al-Malaika, S. and Amir, E. J., *J. Nat. Rubber Res.*, 1986, **1**(2), 104.
13. Kuriakose, B. and De, S. K., *Int. J. Polym. Mater.*, 1986, **11**, 101.
14. Kuriakose, B. and De, S. K., *Polym. Eng. Sci.*, 1985, **25**(10), 630.
15. Tadmor, Z. and Gogos, C. G., *Principles of Polymer Processing*. John Wiley, New York, 1979.
16. Pearson, J. R. A., *Mechanics of Polymer Processing*. Elsevier Applied Science, London, 1985.
17. Cox, A. P. D. and Tenner, R. T., *Polym. Eng. Sci.*, 1980, **20**, 562.
18. Bruker, I. and Blach, G. S., *Polym. Eng. Sci.*, 1989, **29**, 258.
19. Zhu, F. H. and Chen, L. Q., *Polym. Eng. Sci.*, 1991, **31**, 1113.
20. Lee, K. Y., Ph.D. thesis, Polytechnic University, New York.